

Leader-Following Formation Control with Collision Avoidance for Nonholonomic Mobile Robots: Theory and Experiment

Hoang Huy Vu[†], Tan Duy Dang[‡], Nam Hoai Nguyen^{†*}

Abstract—In this paper, the leader-follower formation control and collision avoidance problem for a class of nonholonomic mobile robots (NMRs). The approach involves utilizing observers to estimate the leader's states and the APF method to solve collision avoidance. We proposed a distributed formation controller to achieve the desired formation of NMRs without collision. The Lyapunov function technique is employed to analyze the efficiency of observers and controllers. Numerical simulations and extensive experiments on a group of nonholonomic mobile robots are presented to demonstrate the effectiveness of the theoretical results.

Index Terms—formation control, leader-follower, nonholonomic, collision avoidance

I. INTRODUCTION

With the prompt advancement in science and technology, the trend of enhancing autonomous vehicle systems attracts many researchers. Mobile robots are widely researched and developed for their essential applications in industries, and also in civil demand [1], [2]. In recent years, the formation control of a group of agents has been surging as an active topic for the research community in theories, experiments, and applications due to the advantage of achieving goals with better performance compared with a single robot [3], [4], [5].

Mobile robots with nonholonomic constraints lead to the challenging tasks of designing controllers in the mobile robotics field [6], [7]. Nonholonomic robots intrinsically bear motion limitations originating from their kinematic model, hence some directions of motion are not allowed. The most common kinematic model in literature and practice for the control of mobile robots is the first-order presentation [8], [9], [10]. The reasons are the control problem is easier to solve, the system's dynamics can usually be ignored (by assuming that the actuators are fast, strong, without delay), especially at moderate speeds and the robot design sometimes takes inputs only as reference speeds but not the torque or stimulating electric current. The environment also plays an important role in the problem of controlling mobile robots. For the obstacle-free plane, the tracking problems from point to point or feasible predetermined trajectory are solved in many works with classic, advanced, or intelligent control approaches such as [11], [12], [13]. When there exist obstacles on the plane, or the target is to explore an unknown map, path planning algorithms are introduced to

solve the problems [14], [15]. Nonholonomic systems can be controlled by feedforward controllers [13], [16], where the system's inputs are calculated from the known trajectory, and all kinematic constraints are implicitly considered by trajectory design. However, the use of the open-loop control with only feedforward is hardly applicable in practice as it is not robust to errors in initial system states and other disturbances during operation. Therefore, the closed-loop control scheme is added for practical use, combined with feedforward control, and suitable for most nonholonomic mechanical systems.

Formation control is a technique to form a group of agents into a certain pattern. The reason for researching formation control is the broad promising applications advantaging in faster task execution, the system's robustness, operation in a larger area, and many more. Systems such as NMRs, and UAVs applied formation control can complete complex tasks with a higher success rate and much lower expense than a single complex robot owing to their modularity and flexibility [4], [17]. From the survey paper [18] and reviewed in [19], there are two perspectives of the formation control method: the measurement information perspective and the control mechanism perspective. The first perspective can be categorized into two types: displacement-based methods (Robots can measure their neighbors' relative positions in the common coordinate, then control the relative position automatically), distance-based methods (Robots can measure their neighbors' relative distances through their local coordinate, then control the distances among agents). The second perspective includes roughly four formation control approaches: the behavior-based approach, the virtual structure approach, the potential field-based approach, and the leader-follower approach. In behavior-based control, each robot is imposed with desired behaviors so that the control outcome is the combination of all possible behaviors with weighted relations. This approach meets difficulties because mathematical analysis for complex dynamics of the robot group is not always available. In the virtual structure approach, the requested geometry pattern is considered as a single entity. The simplicity of this approach comes from coordinated group behavior description; however, the virtual structure approach has problems with time-varying group formation. In the artificial potential method, a function called the potential field function will be appropriately selected and its gradient will be utilized for the control design scheme. One significant drawback of this approach is that the global minimum is not guaranteed so the shape of the multi-agent system may not converge to the desired formation.

[†]Department of Automation Engineering, School of Electrical and Electronic Engineering, Hanoi University of Science and Technology (HUST), Hanoi, Vietnam. E-mails: hoang.vh200250@sis.hust.edu.vn.

[‡]Viettel High Technology Industries Corporation, Viettel Group, Ha Noi, Vietnam. Emails: tandd6@viettel.com.vn

*Correspond author. E-mails: nam.nguyenhoai@hust.edu.vn.

In the leader-follower approach, a group of follower agents is expected to follow a (virtual) leader while maintaining desired relative positions and orientations concerning it. The usual assumption is that the information of the leader is known to every follower, but in practice, only a subset of the group can directly get data from it due to the limitations of hardware configuration, and range of connections. Using the communication links among agents, distributed observers for each follower were introduced to estimate the leader's states in [19], [20], [21].

An inevitable problem in formation control of nonholonomic mobile robots is collision avoidance. The APF is a widely used technique for real-time collision avoidance due to its simplicity and effectiveness. Several documents and publications implement algorithms for robotics systems such as [22], [23], [24], [25]. The basis of APF is to define a potential field function such that an object from initial states can reach an aimed point by utilizing the gradient of that potential field function. The shortcomings of the APF method can be listed as the goals non-reachable with nearby obstacles problem, the reach-around local minimum problem. The improvements for those limitations were partly addressed in [26], [27], [28], that the structures of the potential functions were modified or adaptively transformed to manage the repulsive factors affecting the agent near obstacles, but only applied to a single robot and no experiments were conducted to verify the behavior of the robots in the real world. Although APF has been developed and employed in practice for a long time, the combination of formation control with collision avoidance for NMR systems remains an attractive topic.

The main contributions of this paper are listed as follows. Firstly, an alternative approach to integrating the leader-follower formation control method with the repulsive APF function is to achieve the desired formation target of the system of NMRs without collision. Secondly, a modified distributed formation control law is designed based on the observed information of the leader agent. Thirdly, a dynamic gain for repulsive APF function is formulated by the positions of an agent and surrounding objects, with distances between them. Fourthly, The convergence of formation tracking errors is analyzed via Lyapunov theory based on the interaction graph among the leader and follower NMRs. Finally, numerical simulations and extensive experiments in the laboratory are carried out to verify the validity of the proposed control scheme.

II. PRELIMINARIES

A. Notation

The sets of real and complex numbers are denoted by \mathbb{R} and \mathbb{C} , respectively. \mathbf{A}^\top is the transpose of a matrix $\mathbf{A} \in \mathbb{R}^{m \times n}$. The 1-norm, 2-norm of \mathbf{A} are denoted as $\|\mathbf{A}\|_1$, $\|\mathbf{A}\|_2$, respectively. The gradient of the function f is ∇f and its partial derivative to x is $\frac{\partial f}{\partial x}$.

Define a set of state vectors $\mathbf{x}_1, \dots, \mathbf{x}_n \in \mathbb{R}^d$ in vector form as $\text{vec}(\mathbf{x}_1, \dots, \mathbf{x}_n) = [\mathbf{x}_1^\top, \dots, \mathbf{x}_n^\top]^\top \in \mathbb{R}^{dn}$.

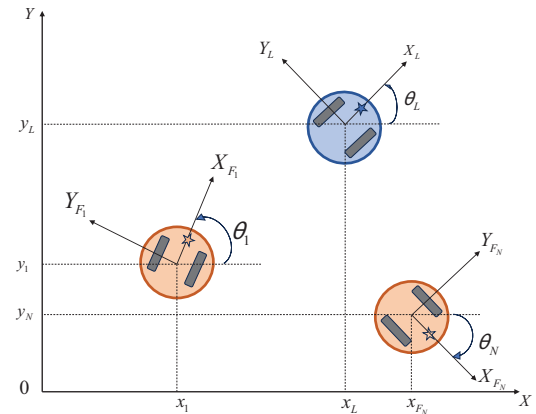


Fig. 1. Global and local coordinates of multi-robot system

For $b \in \mathbb{R}$, we define sign function as follows:

$$\text{sgn}(b) = \begin{cases} -1 & , b < 0 \\ 0 & , b = 0 \\ 1 & , b > 0. \end{cases} \quad (1)$$

For \mathbf{B} is a matrix, $\text{sgn}(\mathbf{B}) = [\text{sgn}(b_{ij})]$.

B. Graph Theory

A network formed by N agents can be represented by a directed graph $\mathcal{G} = \{\mathcal{V}, \mathcal{E}\}$, where $\mathcal{V} = \{1, 2, \dots, N\}$ is the set of nodes and $\mathcal{E} \subseteq \mathcal{V} \times \mathcal{V}$ is the set of edges. The adjacency matrix $\mathbf{A} = (a_{ij})_{N \times N}$ is defined with each nonnegative element $a_{ij} \neq 0$ if $(j, i) \in \mathcal{E}$ and it takes the value 0 otherwise. The Laplacian matrix of \mathcal{G} is denoted with \mathbf{L} which follows the agreement that $l_{ij} = -a_{ij}$ if $i \neq j$ and $l_{ii} = \sum_{j \in N_i} a_{ij}$ for $i = 1, 2, \dots, N$, where $N_i = \{j \in \mathcal{V} \mid (j, i) \in \mathcal{E}\}$ is called the set of neighbors of node i . If $(i, j) \in \mathcal{E} \Leftrightarrow (j, i) \in \mathcal{E}$, \mathcal{G} is called an undirected graph. The graph \mathcal{G} is connected if for each pair of vertices, there exists at least one single path joining them.

For the leader-follower case, consider a system that includes $N + 1$ agents with one leader and N followers. For N followers, the interaction among them can be illustrated by an undirected graph \mathcal{G} . The leader is indexed as 0 (or L). The matrix $\mathbf{B} = \text{diag}[b_1 \dots b_N]$, where $b_i > 0$ if follower i has a direct connection with the leader and $b_i = 0$ otherwise. To simplify further calculations, a pinning matrix $\mathbf{H} = \mathbf{L} + \mathbf{B}$ is defined. We assume that the value of a_{ij}, b_i can only be whether 0 or 1.

Assumption 1: Undirected graph \mathcal{G} is connected and at least one follower has direct connection with the leader.

Lemma 1 ([29]): If \mathcal{G} is an undirected and connected graph, and at least one follower i has direct connection with the leader, such that $b_i = 1$, then H will be a symmetric positive definite matrix.

C. Mobile Robot's Model

Consider a multi-robot system consisting of $N+1$ ($N \geq 2$) nonholonomic mobile robots as shown in Fig. 1. Each agent

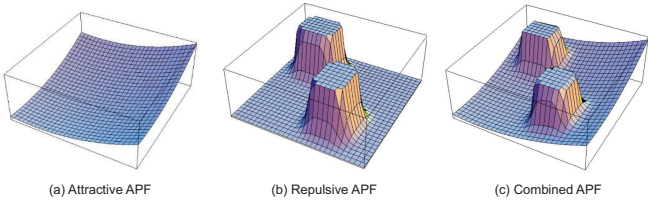


Fig. 2. Three-dimensional APF visualization: (a) - attractive APF; (b) - repulsive potential field; (c) - superposition the two fields.

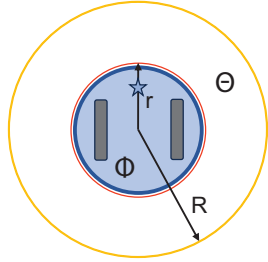


Fig. 3. Detection area (bounded by red and yellow circle) and Collision area (inside red circle)

has the following kinematics model as follows:

$$\begin{aligned}\dot{x}_i &= v_i \cos \theta_i, \\ \dot{y}_i &= v_i \sin \theta_i, \\ \dot{\theta}_i &= \omega_i,\end{aligned}\quad (2)$$

where $x_i, y_i, \theta_i, v_i, \omega_i$ are position, orientation, linear, and angular velocity of i -th agent ($i = 0, 1, \dots, N$), respectively. Denote $\mathbf{q}_i = [x_i \ y_i \ \theta_i]^\top$, $\mathbf{p}_i = [x_i \ y_i]^\top$, $\theta_i \in (-\pi, \pi]$.

Assumption 2: The signals \dot{v}_L, \dot{w}_L are bounded, i.e., $\exists \rho_v, \rho_w > 0$, $\max |\dot{v}_L| \leq \rho_v$ and $\max |\dot{w}_L| \leq \rho_w$.

D. Artificial Potential Field

APF is a method to direct an object to reach a certain position while avoiding obstacles. As in [22], the basic idea of APF is a way of representing a potential energy field, so that the object moves from a higher potential energy position to a lower desired one. Fig. 2. illustrates how APF can be visualized in three-dimensional space.

In the paper, only repulsive APF is investigated to solve the collision avoidance problem. The common way to execute is to select a distance-based repulsive APF function satisfying its value that goes from 0 to $+\infty$ when the distance (between object and obstacle) varies between collision range r and detection range R around an obstacle, then remains 0 if that distance is greater than R (see Fig. . The negative gradient of the function will be implemented in the control law.

III. PROBLEM STATEMENT

We consider the system of nonholonomic mobile robots whose model as in (2). The environment for operation is flat, not inclined, and has obstacles. The leader-isolated robot plays the role of the reference signal which guides the movement of all the following robots. Define the relative position for each follower robot i with respect to the leader

$\Xi_i = [\Xi_{x_i} \ \Xi_{y_i}]^\top$ and the ranges surrounding each object identified by parameters R, r stated in subsection II-D.

The control objective is to design a distributed control law v_i and w_i for all follower mobile robots $i = 1, \dots, N$ so that the formation pattern of the multi-robot system can be achieved without collisions among agents and obstacles.

Objective Control: We formalize the problem as follows: For $i = 1, 2, \dots, N$, the system guarantees that:

- $\|x_L - x_i + \Xi_{x_i}\| + \|y_L - y_i + \Xi_{y_i}\| + \|\theta_L - \theta_i\| \rightarrow 0$, when $t \rightarrow \infty$,
- $\Delta_{a_{ij}}(t) > r, \forall t > 0$, where $\Delta_{a_{ij}} = \|\mathbf{p}_i - \mathbf{p}_j\|$.

IV. CONTROL DESIGN

A. Distributed Observers

The observers based on the communication graph among agents and direct leader's states from certain followers.

Define the neighborhood positions and orientation error variables of the follower i as follows:

$$e_{x_i} = \sum_{m=1}^N a_{im} (\hat{x}_{L_i} - \hat{x}_{L_m}) + a_{i0} (\hat{x}_{L_i} - x_L), \quad (3a)$$

$$e_{y_i} = \sum_{m=1}^N a_{im} (\hat{y}_{L_i} - \hat{y}_{L_m}) + a_{i0} (\hat{y}_{L_i} - y_L), \quad (3b)$$

$$e_{\theta_i} = \sum_{m=1}^N a_{im} (\hat{\theta}_{L_i} - \hat{\theta}_{L_m}) + a_{i0} (\hat{\theta}_{L_i} - \theta_L), \quad (3c)$$

where $\hat{x}_{L_i}, \hat{y}_{L_i}, \hat{\theta}_{L_i}$ are the leader's x coordinate, y coordinate, orientation estimations of robot i , respectively.

The state estimation algorithms for robot i are defined:

$$\dot{\hat{x}}_{L_i} = \frac{1}{\eta_i} \left(-\Gamma_{x_i} e_{x_i} + \sum_{j=1}^N a_{im} \dot{x}_{L_m} + a_{i0} \dot{x}_L \right), \quad (4a)$$

$$\dot{\hat{y}}_{L_i} = \frac{1}{\eta_i} \left(-\Gamma_{y_i} e_{y_i} + \sum_{j=1}^N a_{im} \dot{y}_{L_m} + a_{i0} \dot{y}_L \right), \quad (4b)$$

$$\dot{\hat{\theta}}_{L_i} = \frac{1}{\eta_i} \left(-\Gamma_{\theta_i} e_{\theta_i} + \sum_{j=1}^N a_{im} \dot{\theta}_{L_m} + a_{i0} \dot{\theta}_L \right), \quad (4c)$$

where $\eta_i = a_{i0} + \sum_{m=1}^N a_{im}$ and $\Gamma_{x_i}, \Gamma_{y_i}, \Gamma_{\theta_i}$ are positive constants.

Next, we define the neighborhood linear velocity and angular velocity errors of the follower i as follows:

$$e_{v_i} = \sum_{m=1}^N a_{im} (\hat{v}_{L_i} - \hat{v}_{L_m}) + a_{i0} (\hat{v}_{L_i} - v_L), \quad (5a)$$

$$e_{w_i} = \sum_{m=1}^N a_{im} (\hat{w}_{L_i} - \hat{w}_{L_m}) + a_{i0} (\hat{w}_{L_i} - w_L), \quad (5b)$$

where $\hat{v}_{L_i}, \hat{w}_{L_i}$ are the leader's linear velocity and angular velocity estimations of robot i , respectively.

The velocities estimation algorithms for follower i are:

$$\dot{\tilde{v}}_{L_i} = -\kappa_v e_{v_i} - \sigma_v \operatorname{sgn}(e_{v_i}), \quad (6a)$$

$$\dot{\tilde{w}}_{L_i} = -\kappa_w e_{w_i} - \sigma_w \operatorname{sgn}(e_{w_i}), \quad (6b)$$

where $\kappa_v, \kappa_w > 0$, and $\sigma_v > \rho_v > 0, \sigma_w > \rho_w > 0$.

We define variables $\tilde{\mathbf{x}} = \hat{\mathbf{x}}_L - \mathbf{1}_N \mathbf{x}_L, \tilde{\mathbf{y}} = \hat{\mathbf{y}}_L - \mathbf{1}_N \mathbf{y}_L, \tilde{\theta} = \hat{\theta}_L - \mathbf{1}_N \theta_L, \tilde{\mathbf{v}} = \hat{\mathbf{v}}_L - \mathbf{1}_N \mathbf{v}_L, \tilde{\mathbf{w}} = \hat{\mathbf{w}}_L - \mathbf{1}_N \mathbf{w}_L$, where $\hat{\mathbf{x}}_L = \operatorname{vec}(\hat{x}_{L_i}), \hat{\mathbf{y}}_L = \operatorname{vec}(\hat{y}_{L_i}), \hat{\theta}_L = \operatorname{vec}(\hat{\theta}_{L_i}), \hat{\mathbf{v}}_L = \operatorname{vec}(\hat{v}_{L_i}), \hat{\mathbf{w}}_L = \operatorname{vec}(\hat{w}_{L_i}), \mathbf{e}_x = \operatorname{vec}(e_{x_i}), \mathbf{e}_y = \operatorname{vec}(e_{y_i}), \mathbf{e}_\theta = \operatorname{vec}(e_{\theta_i}), \mathbf{e}_v = \operatorname{vec}(e_{v_i}), \mathbf{e}_w = \operatorname{vec}(e_{w_i}) (i = 1, \dots, N)$.

From (5) and (6), we obtain for n -follower system:

$$\dot{\tilde{\mathbf{v}}} = -\kappa_v \mathbf{H} \tilde{\mathbf{v}} - \sigma_v \operatorname{sgn}(\mathbf{H} \tilde{\mathbf{v}}) - \dot{\mathbf{v}}_L \mathbf{1}_N \quad (7a)$$

$$\dot{\tilde{\mathbf{w}}} = -\kappa_w \mathbf{H} \tilde{\mathbf{w}} - \sigma_w \operatorname{sgn}(\mathbf{H} \tilde{\mathbf{w}}) - \dot{\mathbf{w}}_L \mathbf{1}_N \quad (7b)$$

Lemma 2 ([19]): Suppose that Assumption 1 and 2 hold, under algorithms (4) and (7), $\hat{x}_{L_i}, \hat{y}_{L_i}, \hat{\theta}_{L_i}, \hat{v}_{L_i}, \hat{w}_{L_i}$ converge to the leader's states for $i = 1, \dots, N$.

Proof: We proposed the candidate Lyapunov function:

$$V_1 = \frac{1}{2} \tilde{\mathbf{x}}^\top \mathbf{H}^\top \mathbf{H} \tilde{\mathbf{x}} + \frac{1}{2} \tilde{\mathbf{y}}^\top \mathbf{H}^\top \mathbf{H} \tilde{\mathbf{y}} + \frac{1}{2} \tilde{\theta}^\top \mathbf{H}^\top \mathbf{H} \tilde{\theta} + \frac{1}{2} \tilde{\mathbf{v}}^\top \mathbf{H} \tilde{\mathbf{v}} + \frac{1}{2} \tilde{\mathbf{w}}^\top \mathbf{H} \tilde{\mathbf{w}} \quad (8)$$

By taking the derivative of V_1 with respect to time, one yields:

$$\begin{aligned} \dot{V}_1 &= \tilde{\mathbf{x}}^\top \mathbf{H}^\top \dot{\mathbf{e}}_x + \tilde{\mathbf{y}}^\top \mathbf{H}^\top \dot{\mathbf{e}}_y + \tilde{\theta}^\top \mathbf{H}^\top \dot{\mathbf{e}}_\theta \\ &\quad + \tilde{\mathbf{v}}^\top \mathbf{H} \tilde{\mathbf{v}} + \tilde{\mathbf{w}}^\top \mathbf{H} \tilde{\mathbf{w}} \\ &= \tilde{\mathbf{x}}^\top \mathbf{H}^\top (-\Gamma_x \mathbf{e}_x) \\ &\quad + \tilde{\mathbf{y}}^\top \mathbf{H}^\top (-\Gamma_y \mathbf{e}_y) + \tilde{\theta}^\top \mathbf{H}^\top (-\Gamma_\theta \mathbf{e}_\theta) \\ &\quad + \tilde{\mathbf{v}}^\top \mathbf{H} (-\kappa_v \mathbf{H} \tilde{\mathbf{v}} - \sigma_v \operatorname{sgn}(\mathbf{H} \tilde{\mathbf{v}}) - \dot{\mathbf{v}}_L \mathbf{1}_N) \\ &\quad + \tilde{\mathbf{w}}^\top \mathbf{H} (-\kappa_w \mathbf{H} \tilde{\mathbf{w}} - \sigma_w \operatorname{sgn}(\mathbf{H} \tilde{\mathbf{w}}) - \dot{\mathbf{w}}_L \mathbf{1}_N) \\ &= -\tilde{\mathbf{x}}^\top (\mathbf{H}^\top \Gamma_x \mathbf{H}) \tilde{\mathbf{x}} \\ &\quad - \tilde{\mathbf{y}}^\top (\mathbf{H}^\top \Gamma_y \mathbf{H}) \tilde{\mathbf{y}} - \tilde{\theta}^\top (\mathbf{H}^\top \Gamma_\theta \mathbf{H}) \tilde{\theta} \\ &\quad - \kappa_w \tilde{\mathbf{w}}^\top \mathbf{H}^2 \tilde{\mathbf{w}} - \sigma_w \mathbf{H}^\top \tilde{\mathbf{w}} \operatorname{sgn}(\mathbf{H} \tilde{\mathbf{w}}) - \tilde{\mathbf{w}}^\top \mathbf{H} \tilde{\mathbf{w}} \mathbf{1}_N \\ &\quad - \kappa_v \tilde{\mathbf{v}}^\top \mathbf{H}^2 \tilde{\mathbf{v}} - \sigma_v \mathbf{H}^\top \tilde{\mathbf{v}} \operatorname{sgn}(\mathbf{H} \tilde{\mathbf{v}}) - \tilde{\mathbf{v}}^\top \mathbf{H} \tilde{\mathbf{v}} \mathbf{1}_N \quad (9) \end{aligned}$$

Therein, one can get:

$$\begin{aligned} \dot{V}_1 &\leq -\lambda_{\min}(\mathbf{H}^\top \Gamma_x \mathbf{H}) \|\tilde{\mathbf{x}}\|^2 \\ &\quad - \lambda_{\min}(\mathbf{H}^\top \Gamma_y \mathbf{H}) \|\tilde{\mathbf{y}}\|^2 - \lambda_{\min}(\mathbf{H}^\top \Gamma_\theta \mathbf{H}) \|\tilde{\theta}\|^2 \\ &\quad - \kappa_v \tilde{\mathbf{v}}^\top \mathbf{H}^2 \tilde{\mathbf{v}} - (\sigma_v - \rho_v) \|\mathbf{H} \tilde{\mathbf{v}}\|_1 \\ &\quad - \kappa_w \tilde{\mathbf{w}}^\top \mathbf{H}^2 \tilde{\mathbf{w}} - (\sigma_w - \rho_w) \|\mathbf{H} \tilde{\mathbf{w}}\|_1 \\ &\leq -\lambda_{\min}(\mathbf{H}^\top \Gamma_x \mathbf{H}) \|\tilde{\mathbf{x}}\|^2 - \lambda_{\min}(\mathbf{H}^\top \Gamma_y \mathbf{H}) \|\tilde{\mathbf{y}}\|^2 \\ &\quad - \lambda_{\min}(\mathbf{H}^\top \Gamma_\theta \mathbf{H}) \|\tilde{\theta}\|^2 - \kappa_v \lambda_{\min}(\mathbf{H}^2) \|\tilde{\mathbf{v}}\|^2 \\ &\quad - \kappa_w \lambda_{\min}(\mathbf{H}^2) \|\tilde{\mathbf{w}}\|^2 \quad (10) \end{aligned}$$

The matrix \mathbf{H} is symmetric positive definite, (10) leads to $\dot{V}_1 \leq 0$. Therefore, the estimation variables will converge to the states of the leader. ■

B. Repulsive APF Function

The repulsive APF can be illustrated by the detection region Φ (radius R) and collision region Θ (radius r), as shown in Fig. 3 and be formalized as follows:

$$\Phi = \{\mathbf{p} \in \mathbb{R}^2 : \|\mathbf{p} - \mathbf{p}_0\| \leq R\}, \quad (11)$$

$$\Theta = \{\mathbf{p} \in \mathbb{R}^2 : r \leq \|\mathbf{p} - \mathbf{p}_0\| \leq R\}, \quad (12)$$

where $\mathbf{p} = [x \ y]^\top$ is the coordinates of obstacles.

The repulsive APF is proposed as:

$$V_{a_{ij}} = \left(\min \left\{ 0, \varsigma_{ij} \frac{\Delta_{a_{ij}}^2 - R^2}{\Delta_{a_{ij}}^2 - r^2} \right\} \right)^2, \quad (13)$$

where $\Delta_{a_{ij}}$ is the distance between agent i and j , ς_{ij} is the gain coefficient. Absolutely, partial derivatives of $V_{a_{ij}}$ as follows:

$$\frac{\partial V_{a_{ij}}}{\partial x_i} = \begin{cases} 4\varsigma_{ij} \mathcal{H}(x_i - x_j) & , r < \Delta_a < R, \\ 0 & , \text{other cases}, \end{cases} \quad (14)$$

$$\frac{\partial V_{a_{ij}}}{\partial y_i} = \begin{cases} 4\varsigma_{ij} \mathcal{H}(y_i - y_j) & , r < \Delta_a < R, \\ 0 & , \text{other cases}, \end{cases}$$

$$\text{where } \mathcal{H} = \frac{(R^2 - r^2) (\Delta_{a_{ij}}^2 - R^2)}{(\Delta_{a_{ij}}^2 - r^2)^3}.$$

Assumption 3: There exists an optimal bound of $\overline{\varsigma_{ij}}$ such that partial derivations of repulsive APF function for vertical and horizontal are bounded to generate enough push-back effects, rather than reaching infinite.

C. Distributed Controller

We define the global tracking error with integrating repulsive APF function:

$$E_{x_i} = \hat{x}_{L_i} - x_i + \Xi_i^x - \sum_{j \in S_i} \frac{\partial V_{a_{ij}}}{\partial x_i}, \quad (15a)$$

$$E_{y_i} = \hat{y}_{L_i} - y_i + \Xi_i^y - \sum_{j \in S_i} \frac{\partial V_{a_{ij}}}{\partial y_i}, \quad (15b)$$

$$E_{\theta_i} = \hat{\theta}_{L_i} - \theta_i, \quad (15c)$$

where $\Xi_i = [\Xi_i^x \ \Xi_i^y]$ is the relative desired formation between agent i and leader, S_i is the set of all obstacles around the robot i .

Using the transformation matrix, one can have:

$$\begin{bmatrix} x_{E_i} \\ y_{E_i} \\ \theta_{E_i} \end{bmatrix} = \begin{bmatrix} \cos \theta_i & \sin \theta_i & 0 \\ -\sin \theta_i & \cos \theta_i & 0 \\ 0 & 0 & 1 \end{bmatrix} \begin{bmatrix} E_{x_i} \\ E_{y_i} \\ E_{\theta_i} \end{bmatrix} \quad (16)$$

The control algorithm is proposed as follows:

$$\begin{aligned} v_i &= \hat{v}_{L_i} \cos \theta_{E_i} + \alpha_i x_{E_i}, \\ w_i &= \hat{w}_{L_i} + \beta_i \theta_{E_i} + \frac{\tanh \theta_{E_i}}{\theta_{E_i}} y_{E_i} \hat{v}_{L_i}, \end{aligned} \quad (17)$$

where $\alpha_i, \beta_i, i = 1, \dots, N$ are positive constants.

The update law for gain ς is presented as:

$$\dot{\varsigma}_{ij} = 4\mathcal{H} [E_{x_j} (x_{E_j} - x_{E_i}) + E_{y_j} (y_{E_j} - y_{E_i})] \quad (18)$$

Theorem 1: Consider the NMRs system (2), suppose that Assumptions (1), (2), (3) hold, under control laws (17), update gain laws (18) and estimators (4), system achieve desired formation.

Proof: We propose following candidate Lyapunov function:

$$V_2 = \frac{1}{2} \sum_{i=1}^N x_{E_i}^2 + \frac{1}{2} \sum_{i=1}^N y_{E_i}^2 + \frac{1}{2} \sum_{i=1}^N \theta_{E_i}^2 + \frac{1}{2} \tilde{\mathbf{x}}^\top \mathbf{H}^\top \mathbf{H} \tilde{\mathbf{x}} + \frac{1}{2} \tilde{\mathbf{y}}^\top \mathbf{H}^\top \mathbf{H} \tilde{\mathbf{y}} + \frac{1}{2} \tilde{\boldsymbol{\theta}}^\top \mathbf{H}^\top \mathbf{H} \tilde{\boldsymbol{\theta}} + \frac{1}{2} \tilde{\mathbf{v}}^\top \mathbf{H} \tilde{\mathbf{v}} + \frac{1}{2} \tilde{\mathbf{w}}^\top \mathbf{H} \tilde{\mathbf{w}} + \frac{1}{2} \sum_{i=1}^N \sum_{j \in S_i} \tilde{\varsigma}_{ij}^2. \quad (19)$$

Let $\mathbf{x}_E = \text{vec}(x_{E_i})$, $\mathbf{y}_E = \text{vec}(y_{E_i})$, $\boldsymbol{\theta}_E = \text{vec}(\theta_{E_i})$, $\tilde{\varsigma}_{ij} = \bar{\varsigma}_{ij} - \varsigma_{ij}$.

The derivative of V_2 with respect to time yields:

$$\dot{V}_2 = \sum_{i=1}^N x_{E_i} \dot{x}_{E_i} \sum_{i=1}^N y_{E_i} \dot{y}_{E_i} + \sum_{i=1}^N \theta_{E_i} \dot{\theta}_{E_i} + \tilde{\mathbf{x}}^\top \mathbf{H}^\top \mathbf{H} \dot{\tilde{\mathbf{x}}} + \tilde{\mathbf{y}}^\top \mathbf{H}^\top \mathbf{H} \dot{\tilde{\mathbf{y}}} + \tilde{\boldsymbol{\theta}}^\top \mathbf{H}^\top \mathbf{H} \dot{\tilde{\boldsymbol{\theta}}} + \tilde{\mathbf{v}}^\top \mathbf{H} \dot{\tilde{\mathbf{v}}} + \tilde{\mathbf{w}}^\top \mathbf{H} \dot{\tilde{\mathbf{w}}} - \sum_{i=1}^N \sum_{j \in S_i} \tilde{\varsigma}_{ij} \dot{\tilde{\varsigma}}_{ij}. \quad (20)$$

Based on Lemma 2, one can get:

$$\dot{V}_2 \leq \sum_{i=1}^N x_{E_i} \dot{x}_{E_i} \sum_{i=1}^N y_{E_i} \dot{y}_{E_i} + \sum_{i=1}^N \theta_{E_i} \dot{\theta}_{E_i} - \sum_{i=1}^N \sum_{j \in S_i} \tilde{\varsigma}_{ij} \dot{\tilde{\varsigma}}_{ij} \quad (21)$$

Replace (16), (17), (18) into the above inequality, we attain inequation (22). With the equivalent transformation, one has inequation (23). Using Young's inequality, one will derive (24):

The inequality (24) can be presented in the following form:

$$\dot{V}_2 \leq -\zeta V_2 + \psi \quad (25)$$

Based on Lemma 1, ψ is positive and bounded, thus, $0 \leq \psi \leq \Psi$. Let α_i, β_i satisfy $\varsigma > \frac{\psi}{\Psi}$. As $V_2(t) \geq \Psi$, $\dot{V}_2(t) < 0$ is derived in (25). Thus, $V_2(t) \leq \Psi$ is an invariant set, i.e., if $V_2(0) \leq \Psi$, then $\forall t > 0$, $V_2(t) \leq \Psi$ holds. Therefore, the closed-loop system errors can exponentially converge to a small domain of zero. ■

V. NUMERICAL AND EXPERIMENT RESULTS

In this section, the effectiveness of the proposed control scheme will be verified with numerical simulations.

A. Software in the loop (SIL)

The interaction graph among robots are shown in Fig. 4.

1) Formation control without Collision Avoidance: The initial conditions for the followers and the leader are $q_1(0) = [-1.5 \ 1.5 \ 1]^\top$, $q_2(0) = [-2.5 \ -0.5 \ 0]^\top$, $q_3(0) = [-1 \ -2 \ 1]^\top$, $q_L(0) = [2 \ 0 \ 0.6]^\top$. The desired relative positions of each robot with respect to the leader are selected as $\Xi_1 = [-0.75 \ 0]$, $\Xi_2 = [-1.5 \ 0.75]$, $\Xi_3 = [-1.5 \ -0.75]$. The reference linear velocity and angular velocity for the leader robot is set as $v_L = 0.6 \tanh(t)$, $w_L = 0.5 \sin(\frac{\pi t}{4})$. For the observers, the beginning values are initiated as $\hat{q}_{L_1}(0) = [1 \ 0.2 \ 0.2]^\top$, $\hat{q}_{L_2}(0) = [0.8 \ 0.4 \ 0.8]^\top$, $\hat{q}_{L_3}(0) = [0.9 \ 0.3 \ 0.4]^\top$, $\hat{v}_{L_1}(0) = \hat{v}_{L_2}(0) = \hat{v}_{L_3}(0) = 0.3$, $\hat{w}_{L_1}(0) = \hat{w}_{L_2}(0) = \hat{w}_{L_3}(0) = 0.2$, along with that, the parameters used for observers are $\Gamma_{x_i} = \Gamma_{y_i} = \Gamma_{\theta_i} = 4$, $\kappa_v = \kappa_w = 1.5$, $\sigma_v = \sigma_w = 2$. Next, the parameters for artificial potential function are essentially $R = 0.6$, $r = 0.165$, the initial values for the gains are all 1. The parameters for controllers (36), (37) are $\alpha_i = 1$, $\beta_i = 1$.

Fig. 5 shows trajectories of the system with 4 different controllers in [19], [20], [21] and the proposed controller. The proposed controller generated the smoothest trajectories to the desired geometry pattern.

The criteria function $E(t) = \sum_{i=1}^3 (\|x_i - x_L - \Xi_i^x\|^2 + \|y_i - y_L - \Xi_i^y\|^2 + \|\theta_i - \theta_L\|^2)$ is presented in Fig. 6. Obviously, the graph shape of the selected criteria function with the proposed control scheme monotonously converged to 0 through time and was better than the others.

In Fig. 8 and 7, the inputs and states information of the leader robot could almost be achieved in under 2 seconds.

Define variables $\tilde{e}_{x_i} = x_L - x_i + \Xi_i^x$, $\tilde{e}_{y_i} = y_L - y_i + \Xi_i^y$, $\tilde{e}_{\theta_i} = \theta_L - \theta_i$, $\tilde{e}_{v_i} = v_L - v_i$, $\tilde{e}_{w_i} = w_L - w_i$. In Fig. 9, the formation errors of the system reached close to 0 in a certain interval of time as design expectation. It is shown in Fig. 10 that all the follower robots eventually reached the leader's velocities.

2) Formation control with Collision Avoidance: For simulation's parameters, $\Xi_1 = [-2 \ 1]$, $\Xi_2 = [-1 \ 0]$, $\Xi_3 = [-2 \ -1]$, the reference signals of the leader are $v_L = 0.1$, $w_L = 0.3$, the parameters used for observers are $\Gamma_{x_i} = \Gamma_{y_i} = \Gamma_{\theta_i} = 4$, $\kappa_v = \kappa_w = 1$, $\sigma_v = \sigma_w = 1$, the collision range and detection range are determined by $r = 0.33$, $R = 0.7$ and the parameters for controllers (17) are $\alpha_i = 0.3$, $\beta_i = 0.6$. Two obstacles are in $[0 \ 0]^\top$ and $[-1 \ -0.5]^\top$.

Fig. 11 shows the trajectories of the proposed controller in this scenario.

The distances of every pair of objects in the environment are displayed in Fig. 12. When a robot or an obstacle got in the detection area of another object attached to the repulsive APF, the robot would automatically cooperatively adjust its direction to avoid each other.

The formation errors are shown in Fig. 13, which shows that the robot system roughly needed 25 seconds to form a configuration. This amount of time can be changed by adjusting the size of the detection range.

$$\begin{aligned}
\dot{V}_2 \leq & \sum_{i=1}^N w_i x_{E_i} y_{E_i} - \sum_{i=1}^N v_i x_{E_i} + \sum_{i=1}^N x_{E_i} \cos \theta_i \dot{x}_{L_i} + \sum_{i=1}^N x_{E_i} \sin \theta_i \dot{y}_{L_i} - \sum_{i=1}^N w_i x_{E_i} y_{E_i} \\
& - \sum_{i=1}^N x_{E_i} \cos \theta_i \frac{d}{dt} \left(\sum_{j \in S_i} \frac{\partial V_{a_{ij}}}{\partial x_i} \right) - \sum_{i=1}^N x_{E_i} \sin \theta_i \frac{d}{dt} \left(\sum_{j \in S_i} \frac{\partial V_{a_{ij}}}{\partial y_i} \right) - \sum_{i=1}^N y_{E_i} \sin \theta_i \dot{x}_{L_i} + \sum_{i=1}^N y_{E_i} \cos \theta_i \dot{y}_{L_i} \\
& + \sum_{i=1}^N y_{E_i} \sin \theta_i \frac{d}{dt} \left(\sum_{j \in S_i} \frac{\partial V_{a_{ij}}}{\partial x_i} \right) - \sum_{i=1}^N y_{E_i} \cos \theta_i \frac{d}{dt} \left(\sum_{j \in S_i} \frac{\partial V_{a_{ij}}}{\partial y_i} \right) + \sum_{i=1}^N \theta_{E_i} \dot{\theta}_{L_i} - \sum_{i=1}^N \beta_i \theta_{E_i}^2 \\
& - \sum_{i=1}^N \theta_{E_i} \frac{\tanh \theta_{E_i}}{\theta_{E_i}} y_{E_i} \hat{v}_{E_i} - \sum_{i=1}^N \sum_{j \in S_i} \tilde{\zeta}_{ij} 4 \mathcal{H} [(x_j - x_i) E_{x_i} + (y_j - y_i) E_{y_i}]
\end{aligned} \tag{22}$$

$$\begin{aligned}
\dot{V}_2 \leq & - \sum_{i=1}^N \alpha_i x_{E_i}^2 - \sum_{i=1}^N x_{E_i} (\tilde{v}_{L_i} + v_L \cos \theta_L) + \sum_{i=1}^N x_{E_i} [\cos \theta_i (\dot{x}_{L_i} + v_L \cos \theta_L) + \sin \theta_i (\dot{y}_{L_i} + v_L \sin \theta_L)] \\
& - \sum_{i=1}^N y_{E_i} [\sin \theta_i (\dot{x}_{L_i} + v_L \cos \theta_L) - \cos \theta_i (\dot{y}_{L_i} + v_L \sin \theta_L)] + \sum_{i=1}^N \theta_{E_i} \dot{\theta}_{L_i} + \sum_{i=1}^N \frac{1}{2} (E_{x_i}^2 + E_{y_i}^2) \\
& - \sum_{i=1}^N \beta_i \theta_{E_i}^2 - \sum_{i=1}^N \theta_{E_i} \frac{\tanh \theta_{E_i}}{\theta_{E_i}} y_{E_i} \hat{v}_{E_i} - \sum_{i=1}^N x_{E_i} \left[\cos \theta_i \frac{d}{dt} \left(\sum_{j=1, j \neq i}^{S_i} \frac{\partial V_{a_{ij}}}{\partial x_i} \right) + \sin \theta_i \frac{d}{dt} \left(\sum_{j=1, j \neq i}^{S_i} \frac{\partial V_{a_{ij}}}{\partial y_i} \right) \right] \\
& + \sum_{i=1}^N y_{E_i} \left[\sin \theta_i \frac{d}{dt} \left(\sum_{j=1, j \neq i}^{S_i} \frac{\partial V_{a_{ij}}}{\partial x_i} \right) - \cos \theta_i \frac{d}{dt} \left(\sum_{j=1, j \neq i}^{S_i} \frac{\partial V_{a_{ij}}}{\partial y_i} \right) \right]
\end{aligned} \tag{23}$$

$$\begin{aligned}
\dot{V}_2 \leq & - \min(\alpha_i) \sum_{i=1}^N x_{E_i}^2 + \frac{1}{2} \sum_{i=1}^N x_{E_i}^2 + \frac{1}{2} \sum_{i=1}^N (\tilde{v}_{L_i} + v_L \cos \theta_L)^2 + \frac{1}{2} \sum_{i=1}^N x_{E_i}^2 + \frac{1}{2} \sum_{i=1}^N \cos^2 \theta_i (\dot{x}_{L_i} + v_L \cos \theta_L)^2 \\
& + \frac{1}{2} \sum_{i=1}^N x_{E_i}^2 + \frac{1}{2} \sum_{i=1}^N (\dot{y}_{L_i} + v_L \sin \theta_L)^2 + \frac{1}{2} \sum_{i=1}^N y_{E_i}^2 + \frac{1}{2} \sum_{i=1}^N (\dot{x}_{L_i} + v_L \cos \theta_L)^2 + \frac{1}{2} \sum_{i=1}^N \theta_{E_i}^2 + \frac{1}{2} \sum_{i=1}^N \dot{\theta}_{L_i}^2 \\
& - \min(\beta_i) \sum_{i=1}^N \theta_{E_i}^2 - \frac{1}{2} \sum_{i=1}^N \theta_{E_i}^2 - \frac{1}{2} \min(|v|_{E_i}) \sum_{i=1}^N y_{E_i}^2 + \frac{1}{2} \sum_{i=1}^N x_{E_i}^2 + \frac{1}{2} \sum_{i=1}^N y_{E_i}^2 + \frac{1}{2} \sum_{i=1}^N (x_{E_i}^2 + y_{E_i}^2) \\
& + \sum_{i=1}^N \left[\left(\frac{d}{dt} \sum_{j \in S_i} \frac{\partial V_{a_{ij}}}{\partial x_i} \right)^2 + \left(\frac{d}{dt} \sum_{j \in S_i} \frac{\partial V_{a_{ij}}}{\partial y_i} \right)^2 \right] + \sum_{i=1}^N \sum_{j \in S_i} 8 \tilde{\zeta}_{ij}^2 \mathcal{H} [(x_j - x_i)^2 + (y_j - y_i)^2]
\end{aligned} \tag{24}$$

The velocity errors of every follower with the leader are illustrated in Fig. 14.

With the use of criteria function $E(t)$, the result implementing dynamic gain in the artificial potential function was slightly better than the static one.

B. Hardware in the loop (HIL)

In this section, experiments are conducted to validate the applicable potentiality of the proposed algorithm.

Fig. 16 exhibits the workspace and experimental system, with the main components including a ground control station (PC), a router, 8 cameras and a group of robots.

The hardware configuration of a QBot2e for the testbed is shown in Fig. 17. Each robot has 4 wheels for balance

purpose, but only 2 main big wheels operate when it moves. Mobile robots are equipped with 5 reflective markers for overhead cameras to identify.

The simplified communication structure is presented in Fig. 18

The scenario for the experiment requires 1 leader and 2 followers, 2 obstacles. The graph represents connection among agents are in Fig. 19. The collision radius r is 0.165 (QBot radius), detection radius R is 0.9.

Fig. 20 describes the trajectories of all QBot2e robots in 100 seconds. Robots' behaviors achieve the desired formation. What can be indicated is that the follower robots must cross each other to reach the other side of the obstacles, but they eventually complete the transition successfully.

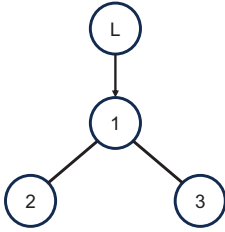


Fig. 4. Connection graph for formation control simulation

Fig. 21 displays distances in time of all pairs of objects in ground plane. Some objects were intentionally placed inside one's detection range from the start. However, after over 40(s), most distances were larger than the detection range, which indicated that robots with the repulsive APF tended to extend their distances among other to the near detection range. Consequently, no pair of agents could approach near collision range, which means no collisions occurred.

In Fig. 22, the errors of input observers promptly converged to 0, then remained close to that value in the whole process. In Fig. 23, the errors of state observers also quickly converged to 0 and continually stayed close to the horizontal axis. It should be noticed that at some moments, specifically at 20 and 60 seconds, the estimation errors of the leader's orientation went down rapidly and then surged swiftly back to 0.

The errors of formation positions and orientations in Fig. 24 illustrate that the multi-robot system was automatically transformed into goal formation.

The velocities of all agents are shown in Fig. 25. The leader's linear velocity and angular velocity gradually reached to reference value without overshooting. With the follower robots, they experienced a variation of velocities in the first 65(s) as they had to move properly across the other and the obstacles. Afterward, all velocities converged to the leader's velocities as the multi-robot system achieved the formation requirement.

REFERENCES

- [1] F. Rubio, F. Valero, and C. Llopis-Albert, "A review of mobile robots: Concepts, methods, theoretical framework, and applications," *International Journal of Advanced Robotic Systems*, vol. 16, no. 2, 2019.
- [2] J. Kramer and M. Scheutz, "Development environments for autonomous mobile robots: A survey," *Autonomous Robots*, vol. 22, no. 2, pp. 101–132, Feb 2007.
- [3] H. Du, G. Wen, Y. Cheng, Y. He, and R. Jia, "Distributed finite-time cooperative control of multiple high-order nonholonomic mobile robots," *IEEE Transactions on Neural Networks and Learning Systems*, vol. 28, no. 12, pp. 2998–3006, 2017.
- [4] Y. Gottlieb and T. Shima, "Uavs task and motion planning in the presence of obstacles and prioritized targets," *Sensors*, vol. 15, no. 11, pp. 29 734–29 764, 2015.
- [5] E. Mehrabi, H. A. Talebi, M. Zareinejad, and I. Sharifi, "Cooperative control of manipulator robotic systems with unknown dynamics," in *2015 International Conference on Advanced Robotics (ICAR)*, 2015, pp. 401–406.
- [6] I. Kolmanovsky and N. McClamroch, "Developments in nonholonomic control problems," *IEEE Control Systems Magazine*, vol. 15, no. 6, pp. 20–36, 1995.
- [7] A. D. Luca and G. Oriolo, *Modelling and Control of Nonholonomic Mechanical Systems*. Vienna: Springer Vienna, 1995, pp. 277–342.
- [8] W. Kowalczyk and K. Kozlowski, "Leader-follower control and collision avoidance for the formation of differentially-driven mobile robots," in *2018 23rd International Conference on Methods & Models in Automation & Robotics (MMAR)*, 2018, pp. 132–137.
- [9] S. Mastellone, D. M. Stipanović, C. R. Graunke, K. A. Intlekofer, and M. W. Spong, "Formation control and collision avoidance for multi-agent non-holonomic systems: Theory and experiments," *The International Journal of Robotics Research*, vol. 27, no. 1, pp. 107–126, 2008.
- [10] X. Yu and L. Liu, "Distributed formation control of nonholonomic vehicles subject to velocity constraints," *IEEE Transactions on Industrial Electronics*, vol. 63, no. 2, pp. 1289–1298, 2016.
- [11] R. R. Carmona, H. G. Sung, Y. S. Kim, and H. A. Vazquez, "Stable pid control for mobile robots," in *2018 15th International Conference on Control, Automation, Robotics and Vision (ICARCV)*, 2018, pp. 1891–1896.
- [12] N. T. Binh, N. A. Tung, D. P. Nam, and N. H. Quang, "An adaptive backstepping trajectory tracking control of a tractor trailer wheeled mobile robot," *International Journal of Control, Automation and Systems*, vol. 17, no. 2, pp. 465–473, Feb 2019.
- [13] V. De Oliveira, E. De Pieri, and W. Lages, "Feedforward control of a mobile robot using a neural network," in *Smc 2000 conference proceedings. 2000 ieee international conference on systems, man and cybernetics. 'cybernetics evolving to systems, humans, organizations, and their complex interactions' (cat. no.0*, vol. 5, 2000, pp. 3342–3347 vol.5.
- [14] O. Khatib, "Real-time obstacle avoidance for manipulators and mobile robots," in *Proceedings. 1985 IEEE International Conference on Robotics and Automation*, vol. 2, 1985, pp. 500–505.
- [15] J. R. Sánchez-Ibáñez, C. J. Pérez-del Pulgar, and A. García-Cerezo, "Path planning for autonomous mobile robots: A review," *Sensors*, vol. 21, no. 23, 2021.
- [16] I.-W. Park, J.-O. Kim, M.-H. Oh, and W. Yang, "Realization of stabilization using feed-forward and feedback controller composition method for a mobile robot," *International Journal of Control, Automation and Systems*, vol. 13, no. 5, pp. 1201–1211, Oct 2015.
- [17] Z. Qu, J. Wang, and R. A. Hull, "Cooperative control of dynamical systems with application to autonomous vehicles," *IEEE Transactions on Automatic Control*, vol. 53, no. 4, pp. 894–911, 2008.
- [18] K.-K. Oh, M.-C. Park, and H.-S. Ahn, "A survey of multi-agent formation control," *Automatica*, vol. 53, pp. 424–440, 2015.
- [19] Z. Miao, Y.-H. Liu, Y. Wang, G. Yi, and R. Fierro, "Distributed estimation and control for leader-following formations of nonholonomic mobile robots," *IEEE Transactions on Automation Science and Engineering*, vol. 15, no. 4, pp. 1946–1954, 2018.
- [20] P. Lu, H. Wang, F. Zhang, W. Yu, and G. Chen, "Formation control of nonholonomic mobile robots using distributed estimators," *IEEE Transactions on Circuits and Systems II: Express Briefs*, vol. 67, no. 12, pp. 3162–3166, 2020.
- [21] Q. Lu, Z. Miao, D. Zhang, L. Yu, W. Ye, S. X. Yang, and C.-Y. Su, "Distributed leader-follower formation control of nonholonomic mobile robots," *IFAC-PapersOnLine*, vol. 52, no. 15, pp. 67–72, 2019, 8th IFAC Symposium on Mechatronic Systems MECHATRONICS 2019.
- [22] H. Choset, K. Lynch, S. Hutchinson, G. Kantor, W. Burgard, L. Kavraki, and S. Thrun, *Principles of Robot Motion: Theory, Algorithms, and Implementations*. MIT Press, May 2005.
- [23] H. M. Jayaweera and S. Hanoun, "A dynamic artificial potential field (d-apf) uav path planning technique for following ground moving targets," *IEEE Access*, vol. 8, pp. 192 760–192 776, 2020.
- [24] A. Lazarowska, "Discrete artificial potential field approach to mobile robot path planning," *IFAC-PapersOnLine*, vol. 52, no. 8, pp. 277–282, 2019, 10th IFAC Symposium on Intelligent Autonomous Vehicles IAV 2019.
- [25] Z. Pan, C. Zhang, Y. Xia, H. Xiong, and X. Shao, "An improved artificial potential field method for path planning and formation control of the multi-uav systems," *IEEE Transactions on Circuits and Systems II: Express Briefs*, vol. 69, no. 3, pp. 1129–1133, 2022.
- [26] C. Kuang, L. Li, and Q. Geng, "Formation control and collision avoidance of nonholonomic mobile robots," in *2021 5th CAA International Conference on Vehicular Control and Intelligence (CVCI)*, 2021, pp. 1–6.

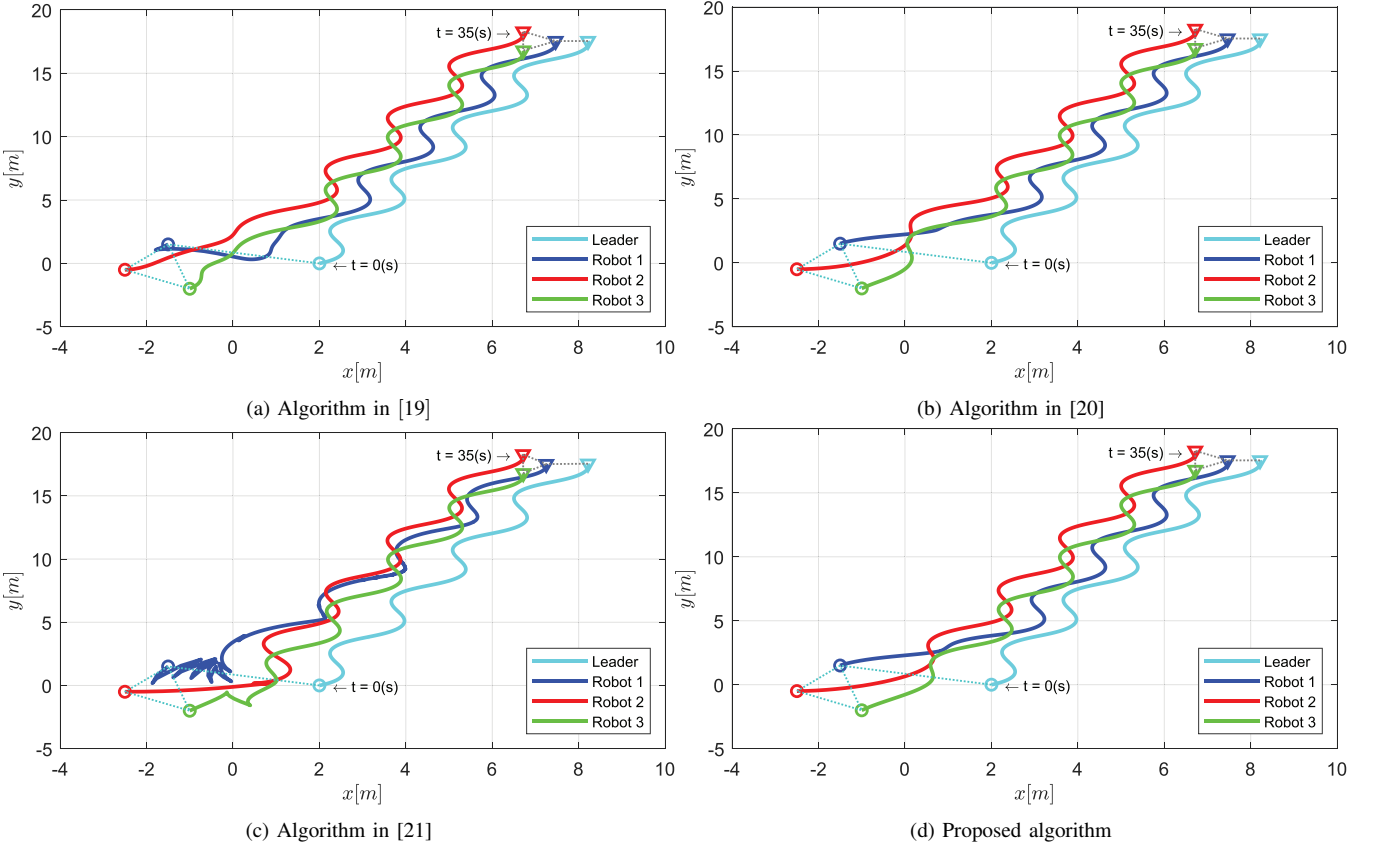


Fig. 5. Trajectories of multi-robot system with different control schemes.

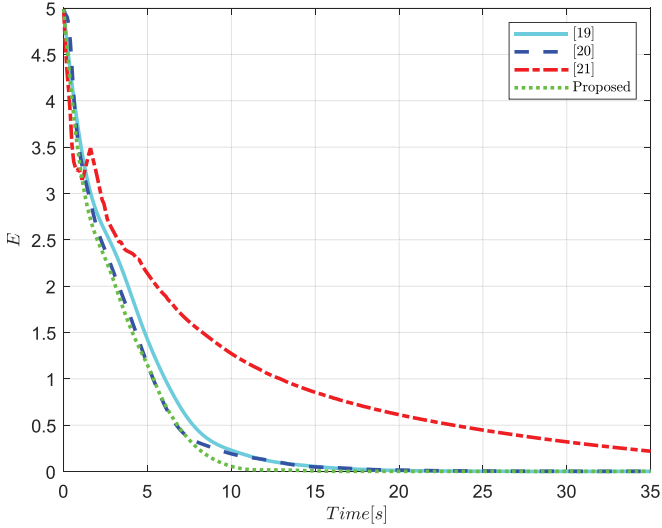


Fig. 6. Comparison results of controllers in formation control simulation.

- [27] F. Bounini, D. Gingras, H. Pollart, and D. Gruyer, "Modified artificial potential field method for online path planning applications," in *2017 IEEE Intelligent Vehicles Symposium (IV)*, 2017, pp. 180–185.
- [28] L. Zhou and W. Li, "Adaptive artificial potential field approach for obstacle avoidance path planning," in *2014 Seventh International Symposium on Computational Intelligence and Design*, vol. 2, 2014, pp. 429–432.
- [29] F. Lewis, H. Zhang, K. Hengster-Movric, and A. Das, *Cooperative Control of Multi-Agent Systems: Optimal and Adaptive Design Approaches*. Springer Publishing Company, Incorporated, 2014.

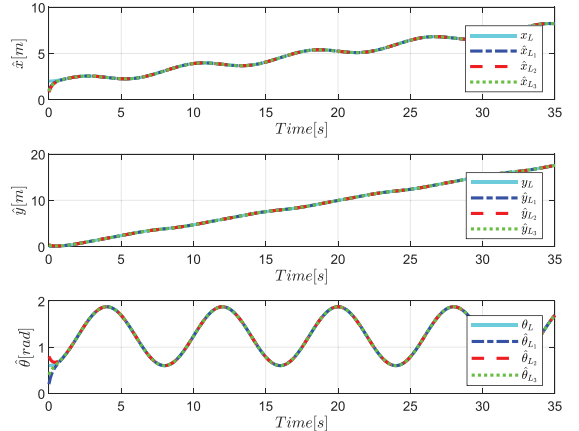


Fig. 7. Estimated leader's states in formation control simulation.

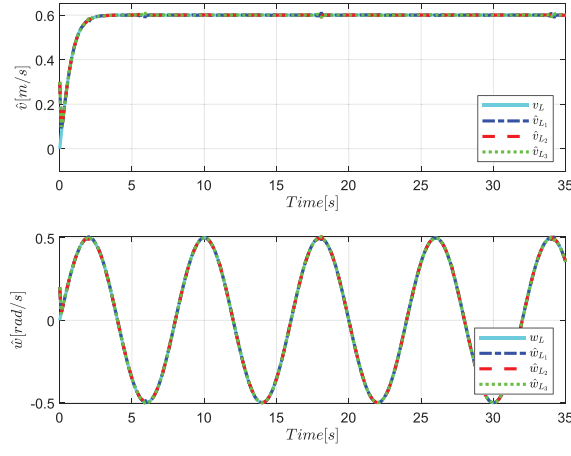


Fig. 8. Estimated leader's inputs in formation control simulation.

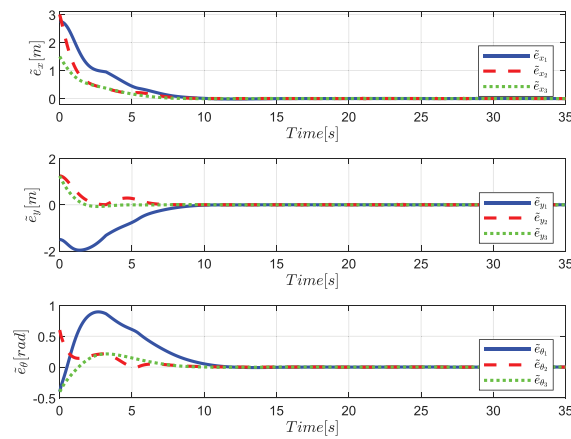


Fig. 9. Formation state errors in formation control simulation.

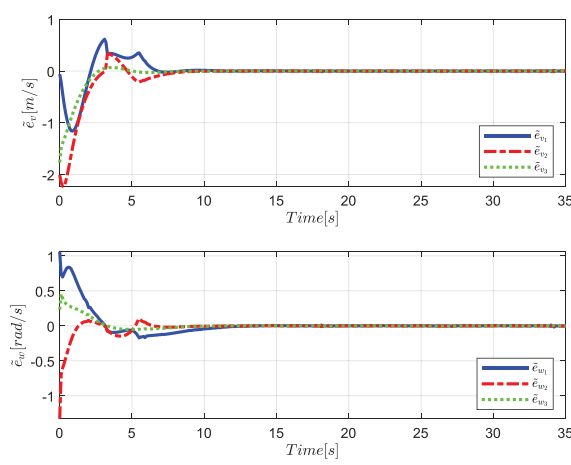


Fig. 10. Formation input errors in formation control simulation.

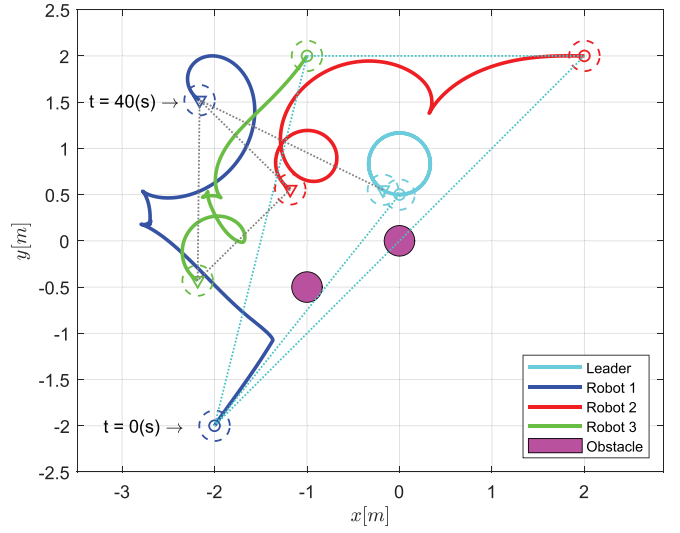


Fig. 11. Trajectories of multi-robot system in formation control with collision avoidance simulation.

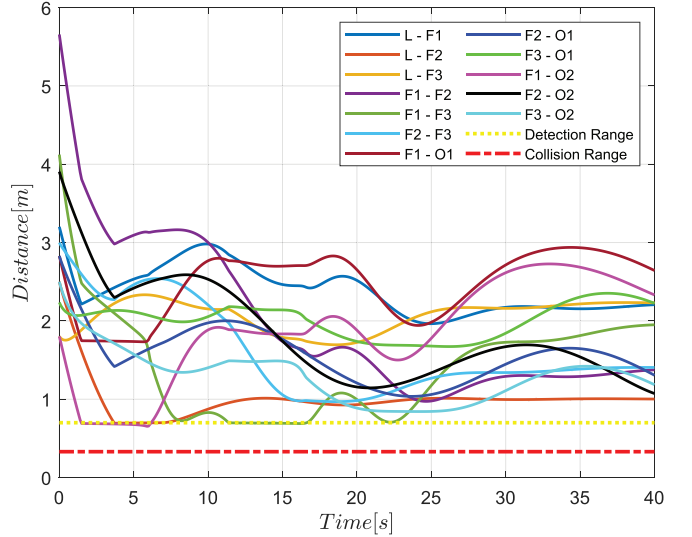


Fig. 12. Distances of all pairs of objects in formation control with collision avoidance simulation.

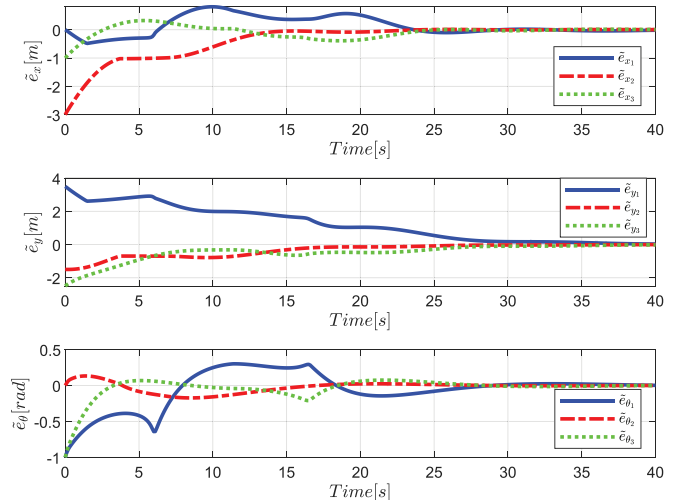


Fig. 13. Formation state errors in formation control with collision avoidance simulation.

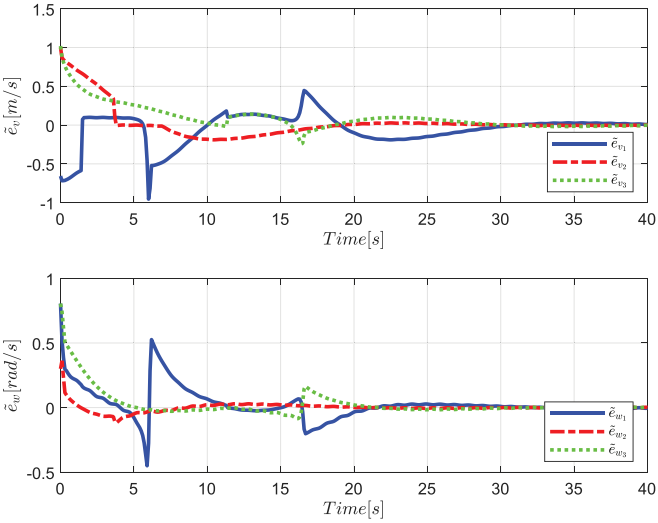


Fig. 14. Formation input errors in formation control with collision avoidance simulation.

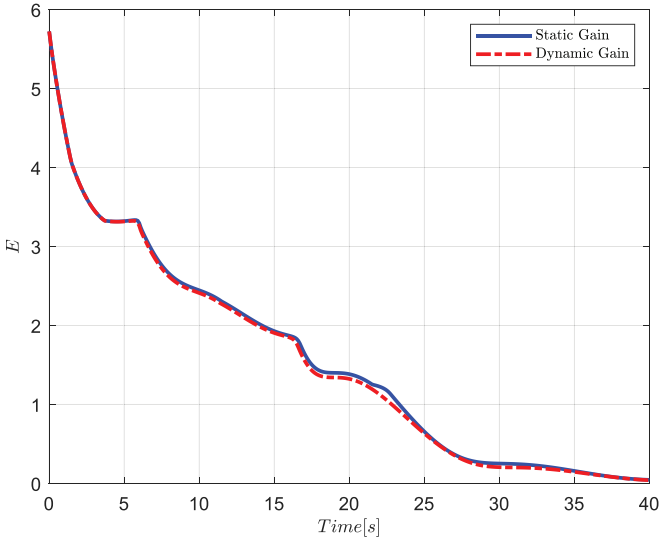


Fig. 15. Comparison of static gain and dynamic gain for the repulsive APF function in formation control with collision avoidance.

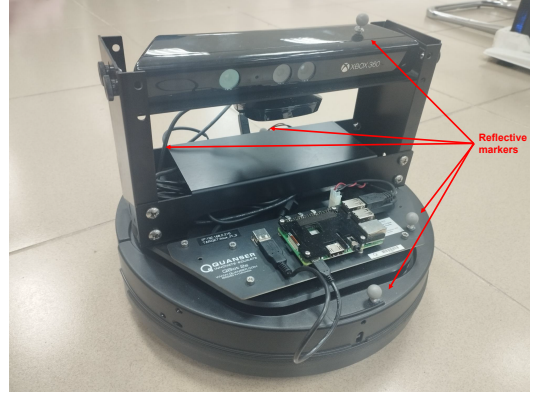


Fig. 17. QBot2e robot with reflective markers (red arrow).

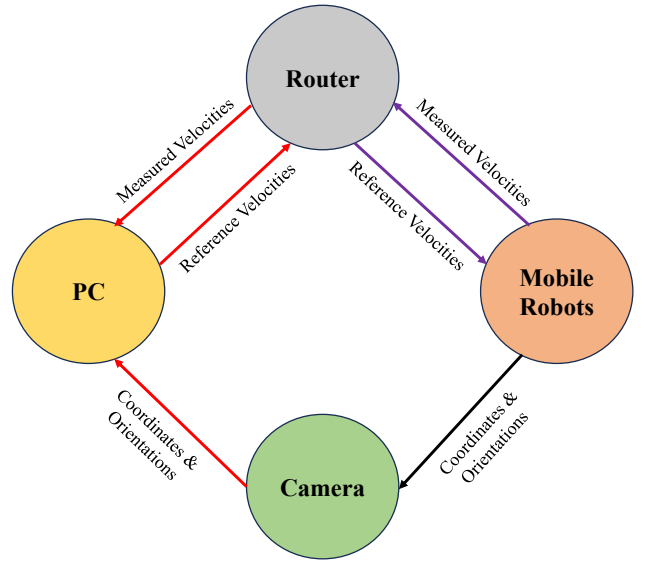


Fig. 18. Communication flow of Control system (red - Ethernet, purple - WiFi, and back - reflective signals from Qbot).

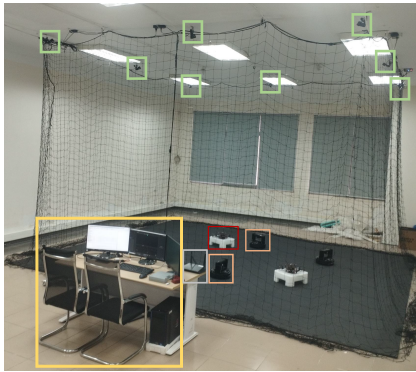


Fig. 16. Experiment Workspace: PC (yellow), Camera (green), Router (gray), Qbot/Agent (orange), Obstacle (red).

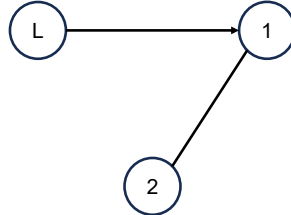


Fig. 19. Connection graph for experiment.

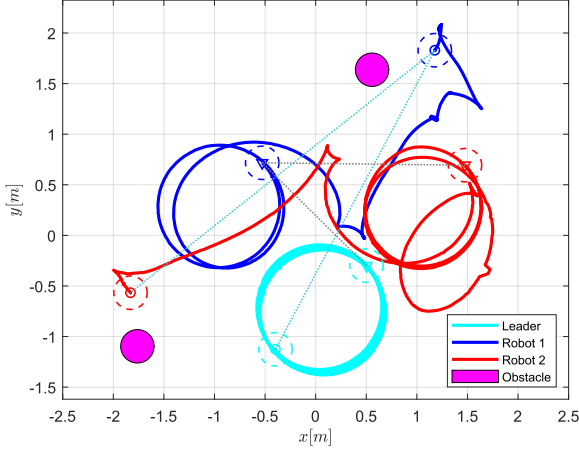


Fig. 20. Trajectories of multi-robot system in experiment.

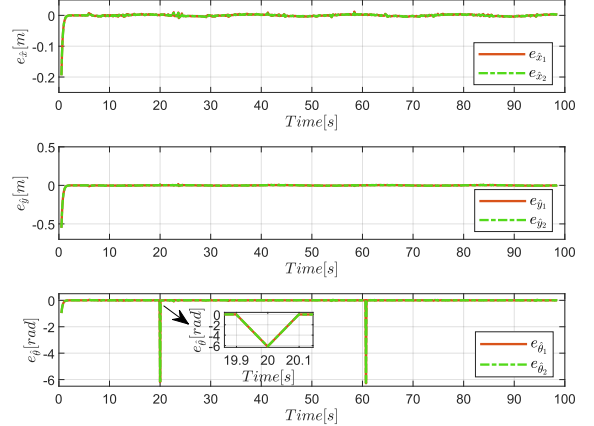


Fig. 23. Estimated leader's state errors in experiment.

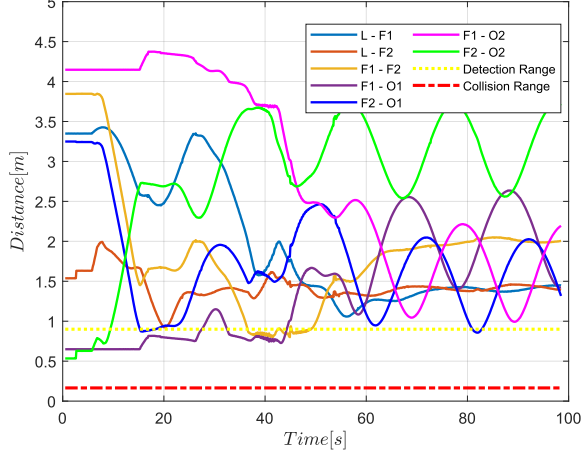


Fig. 21. Distances of all pairs of objects in experiment.

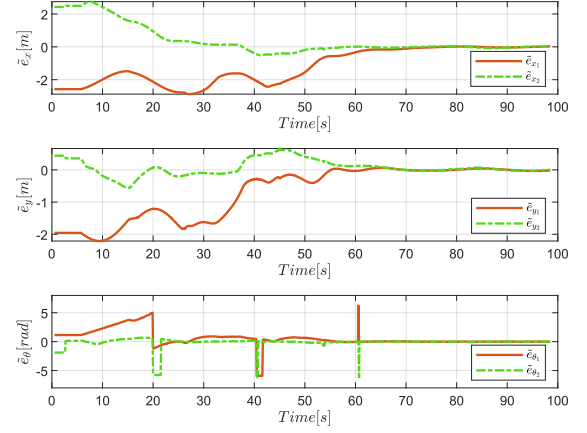


Fig. 24. Formation state errors in experiment.

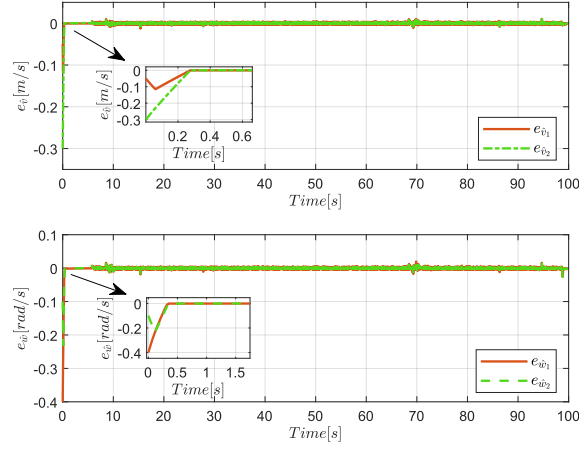


Fig. 22. Estimated leader's input errors in experiment.

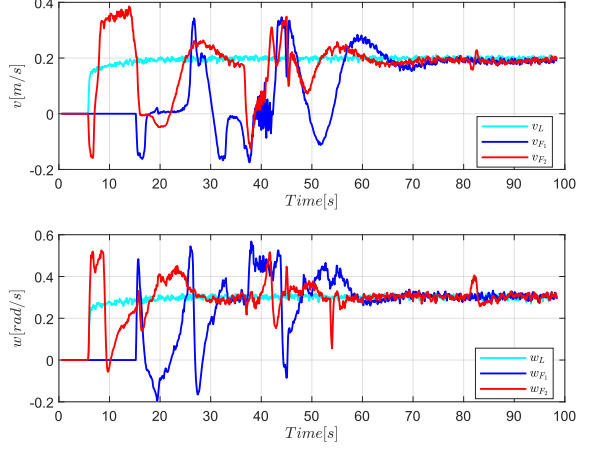


Fig. 25. Velocities of all agents in experiment.